Microwave Observations of the Quiet Sun

Kiyoto Shibasaki
Nobeyama Radio Observatory, Minamimaki, Minamisaku, Nagano 384-1305, Japan
E-mail: shibasaki@nro.nao.ac.jp

Abstract

Recent quiet sun observations in microwave regions are reviewed. In the review, the mechanism of radio emission (thermal free-free) from the quiet sun and atmosphere models of the quiet sun are summarized. The models are compared with the observations of the frequency spectrum of the disk center brightness temperature and of the center-to-limb variations. Then the performances and limitations of the Nobeyama Radioheliograph (NoRH) for studies of the quiet sun are summarized. By stressing the results from the NoRH, several observational features of the quiet sun are summarized. Coronal holes and the polar cap brightening are particularly interesting subjects. It is shown that the NoRH is a powerful tool for quiet sun studies.

Key words: Sun: quiet sun — Sun: microwave — Sun: atmosphere

1. Introduction

Observations of the quiet sun have several aspects in solar physics: sounding the interior of the Sun, studies of the atmosphere, heating mechanism of the corona, solar-cycle variations, and so on. Microwave observations can diagnose the atmosphere at the levels of upper chromosphere, transition region, and lower corona. Low temperature plasma in the corona such as dark filaments can be detected as absorption on the disk and as emission above the limb. In the microwave region, there are no line emissions. This is a severe limitation to the microwave observations of the Sun. Only the integrated nature of the atmosphere can be measured. Brightness temperature distributions, their temporal behaviors, wide band microwave spectra and circular polarization information are the observables. Multi-frequency observations can be a very powerful tool to differenciate the measured data to get physical parameters of the atmosphere. Combination of the microwave observation with other observations such as x-ray, EUV, and optical are also very powerful. Due to its simple emission mechanism, microwave observations are useful to test the atmosphere models.

Spatial resolution is another limitation of microwave observation due to longer wavelength. We need large radio interferometers to get high spatial resolution. In the case of the radio interferometer, image quality or dynamic range depends on how accurately we can calibrate phases and amplitudes and depends on the available number of antennas. As the Sun has complicated structures on the extended disk and they are variable in time, synthesizing images is a difficult task. These limit the subjects to be studied with interferometer data.

In this paper, we define the "quiet sun" as the area outside active regions on the solar disk. Active regions are compact areas with enhanced brightness. So, the quiet sun includes coronal holes and dark filaments / prominences. Transient activities in the quiet sun such as X-ray bright points in coronal holes are not discussed here. However, due to recent increase of sensitivities of the instruments, it became clear that even in quiet areas, many transient activities are going on.

In the following section, I would like to summarize the thermal free-free emission mechanism to understand the observed features in the quiet sun. In sections 3 and 4, current atmospheric models of the quiet sun are reviewed in conjunction with the radio brightness temperature values and center-to-limb variations. In section 5, the instrument summary of the Nobeyama Radioheliograph and its performances are presented focussing on the quiet sun studies. In section 6, recent works on the observed features of the quiet sun are reviewed.

2. Radio Emission from the Quiet Sun

Several radio emission mechanisms are active in the Sun. Main mechanisms are thermal free-free, thermal gyroresonance, and non-thermal gyro-synchrotron. In the quiet sun, thermal free-free is the main emission mechanism

in the microwave region away from sunspots. Absorption coefficient (κ) of the ionized gas is given as follows (the following equations are from Dulk 1985).

$$\begin{aligned} \kappa &= 9.78 \times 10^{-3} \times N_e/(f^2 T^{3/2}) \sum Z_i^2 N_i \\ &\quad \times (18.2 + ln(T^{3/2}) - ln(f)) \quad : (T < 2 \times 10^5 K) \\ or &\quad \times (24.5 + ln(T) - ln(f)) \quad : (T > 2 \times 10^5 K) \end{aligned}$$

Optical depth (τ) and the brightness temperature (T_b) of the ionized gas are expressed using the absorption coefficient.

$$\begin{aligned} \tau &= \int \kappa dl \\ T_b &= \int T e^{-\tau} d\tau \end{aligned}$$

Where,
- T : temperature
- l : length along the line of sight
- N_e : electron density
- N_i : ion density
- Z_i : ion charge
- f : observing frequency

Cgs-units are used in the above expressions. Radio flux (S) is the energy flux per second, per unit bandwidth and per unit area. It relates with the brightness temperature as follows:

$$S = 2k_B/\lambda^2 \int T_b d\Omega \quad \text{(integration over the source or the area)}$$

where, k_B is the Boltzmann's constant and λ is the observing wavelength. The unit of flux density is expressed in $erg/sec/cm^2/Hz$. In solar radio observations, we use the solar flux unit ($1 s.f.u. = 10^{-19} erg/sec/cm^2/Hz = 10^4 Jy$). The total flux of the quiet sun integrated over the solar disk at 17 GHz is around 600 $s.f.u.$

Brightness temperature of the quiet sun at the disk center can be calculated by integrating the above equation. Assuming a stratified model atmosphere we can obtain the temperature, density, and ionization degree distribution as a function of height above the photosphere. Using the model, we calculate the absorption coefficient distribution and then optical depth distribution. Temperature is now expressed as a function of optical depth, and then the integration can be performed. Away from the disk center, line of sight distance increases as a function of $1/cos(\theta)$, where θ is the elongation angle from the disk center. Near the limb, the curvature of the stratified atmosphere needs to be taken into account. In this way, the center to limb variation of the brightness temperature of the quiet sun can be calculated using the above set of equations. Absolute values of the disk center brightness temperature as a function of the observing frequency is one way of testing the model of the atmosphere. Observation of the center to limb variation is another way of testing the model. Generally speaking, limb brightening is expected in the stratified atmosphere model because the temperature is higher at higher altitude.

In case of a plasma cloud sitting above the quiet sun, observed brightness temperature is the combination of that of the quiet sun (T_{bo}) and the contribution from the plasma cloud. Assuming that the temperature of the cloud is uniform over the cloud, a simple two-layer model is used.

$$T_b = T_{bo} e^{-\tau_c} + \int T_c e^{-\tau} d\tau$$

where,

- τ_c : optical depth of the cloud($= \int \kappa dl$)
- T_c : cloud temperature

In an optically thin cloud,

$$T_b = T_{bo} + T_c \tau_c.$$

In an optically thick cloud,

$$T_b = T_c.$$

To estimate the opacity, we need spectral information of radio sources or other measurements such as optical, soft x-ray and EUV. Using the above equations, we can determine the parameters of the plasma cloud in the corona.

Optically thick dark filaments / prominences are normally observed as absorption on the disk and as emission above the limb. The observed brightness temperature is the temperature of the filaments or the prominences themselves. Their brightness temperature should be the same both on and off the disk. If the temperature of the cloud is close to that of the quiet sun, we cannot detect the filament on the disk. Due to the filamentary structure in the dark filament, the observation beam is not entirely filled with plasma. The filling factor modifies the observed brightness. We cannot get the filling factor by radio observation only. We need to assume or rely on other observations. This may influence the interpretation of the observed brightness temperature.

Hot plasma contained in coronal loops in quiet areas or in active regions is often optically thin. From the soft x-ray diagnostics, temperature and emission measure are deduced for the coronal loops. From these values, we can calculate the radio brightness temperature and the flux. Sometimes, the observed radio flux exceeds the calculated one. This is due to the fact that soft x-ray cannot detect large emission measure from the lower temperature below a couple of million degrees, while radio opacity increases as the temperature decreases. Discrepancies are often interpreted as the existence of lower temperature plasma. In the optically thin case, excess brightness temperature depends on the plasma temperature as:

$$\triangle T_b \quad \propto \quad 1/\sqrt{T_c},$$

which is rather insensitive.

3. Atmosphere Models

Height structure of the solar atmosphere has been extensively studied mainly based on the result of UV/EUV observations. Semi-empirical atmosphere models were proposed by Vernazza, Avrett and Loeser (VAL model, 1981) and by Fontenla, Avrett and Loeser (FAL model, 1993). These are one-dimensional, plane-parallel and hydrostatic models. They assumed energy balance of heat flux from the corona and radiation loss. In the VAL model, a temperature plateau was predicted around 20,000 K. However, such a temperature plateau means a density plateau due to the hydrostatic assumption. This causes an opacity increase around 20,000 K and results in higher brightness temperature of the quiet sun in the microwave region that is not observed. In the FAL model, particle diffusion in the region of steep temperature gradient is included and results in no plateau. The FAL model is more realistic than the VAL model so far as the microwave brightness temperature is concerned.

Measurements of absolute values of the brightness temperatures of the quiet sun are important to test the model atmospheres. Accurate measurements were done by Zirin et al. (1991) at the frequency range of $1.4 \sim 18$ GHz. They used a large single dish (27-m diameter) to make the beam smaller than the solar disk. Antenna temperatures were calibrated using the Moon as the reference. They found a large discrepancy between the observed and the calculated brightness temperature using the VAL model. They found a rather simple relation between the brightness temperature (T_b in K) and the frequency (f in GHz).

$$T_b \quad = \quad A f^{-2.1} + T_{chrom}$$

Where, $A = 140{,}077$ K and $T_{chrom} = 10{,}880$ K. The first term is interpreted that the as the optically thin coronal contribution and the second term as the optically thick chromospheric contribution. This relation holds at lower than 10 GHz. In this interpreration, no transition region component contributes to the brightness. At higher frequencies, a more structually detailed atmosphere model needs to be taken into account. This measurement was done around the solar activity minimum. Bastian et al. (1996) measured the quiet sun brightness temperature by the similar way to that of the Zirin et al. (1991) at 15 and 23 GHz. They measured in 1992 when the solar activity was high. Their value at 15 GHz was higher than that of the Zirin et al. The difference is interpreted as the result of the increased coronal contribution due to the higher solar activity. They compared their result and the result by Zirin et al. with VAL and FAL models. They showed that better fits could be found when they use the model atmosphere proposed by Avrett (1995) which satisfy the existence of CO bands. However, it does not fit well with the lower frequencies.

The calculated quiet sun brightness temperature based on FAL model (C) is plotted in Figure 1. In the figure, a coronal contribution is added by the empirical formula by Zirin et al. (1991). The measured values by Zirin et al. (1991) and Bastian et al. (1996) are also plotted.

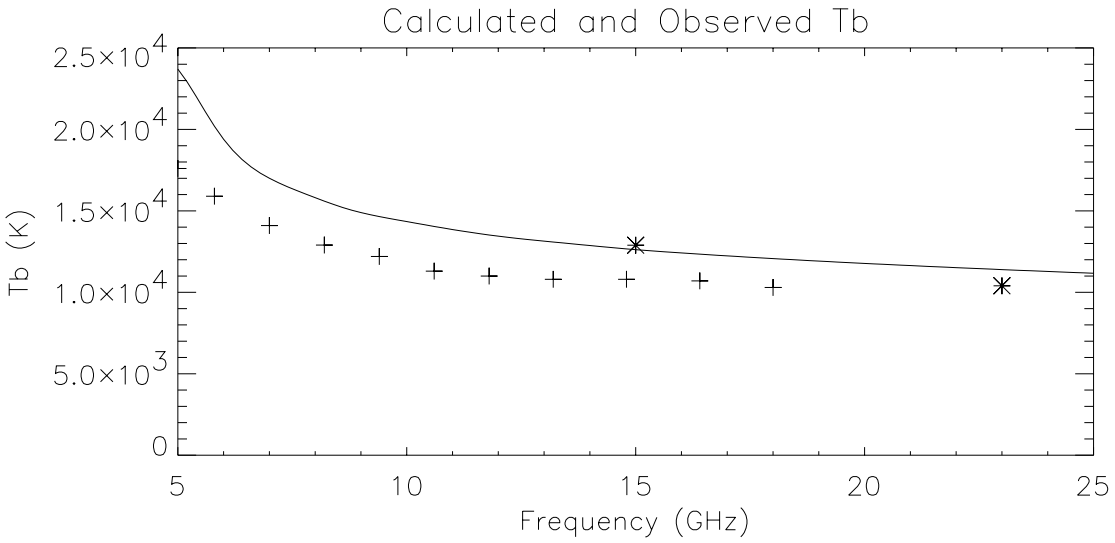

Fig. 1.. Frequency spectrum of the calculated radio brightness based on the FAL-C model (solid line, Fontenla et al., 1993) and the observed brightness (+ Zirin et al., 1991, * Bastian et al., 1996)

4. Center-to-Limb Variation

Measurements of center-to-limb variation of the brightness temperature are another way of testing the model atmosphere as mentioned in the section 3. The path length increase causes an opacity increase. As the temperature is an increasing function of the height above the chromosphere, limb brightening is expected in the case of a plane-parallel atmosphere model. Figure 2 shows the calculated center to limb variation at 17 GHz using the FAL model. In the calculation, the extreme limb is avoided for simplicity.

In actual measurements, there are many disturbing factors. First, the real solar surface is not everywhere quiet sun. Especially, active regions and other features stay longer near the limb because of the projection effect. We need to select the time when the Sun is really quiet. Second is associated with observing instruments. We need large telescopes for such measurements to get sharp beams. However, large telescopes tend to have an extended error sidelobe surrounding the sharp main beam. The error sidelobe is the result of the surface roughness. Because the error sidelobe is extended and also the solar disk is extended, output signals near the limb are strongly distorted. This effect can be estimated by observing the Moon. Difference between the lunar observation and the solar observation can result from the influence of the temperature distribution of the telescope due to the large heat input from the Sun during the observation. Careful treatment is required. Radio interferometric measurement of the center to limb variation requires good baseline length coverage, from short to long in 2-D. And also good phase and amplitude calibrations are essential because of the large brightness jump at the limb.

Restorations are necessary to estimate the real distribution both for large single dish observations and for interferometric observations. This introduces ambiguity in interpreting the observed profiles. Limb brightening and limb darkening is highly dependent on the restorations applied.

Submillimeter observations of the quiet sun by Lindsey et al., (1995) using the JCMT telescope show clear limb brightening after the error beam correction. The center-to-limb variation was more enhanced than the calculated one using the VAL model. In ontrast, the Nobeyama Radioheliograph shows less brightening in E-W and enhanced brightening in N-W. This will be discussed in section 6.

5. Nobeyama Radioheliograph for Quiet Sun Studies

The Nobeyama Radioheliograph (NoRH) is a radio interferometer dedicated for solar observations (Nakajima et al., 1994). The main purpose of the construction of NoRH was to study high-energy phenomena associated with solar flares. However, it became clear that NoRH is also a good instrument for the study of quiet phenomena on the

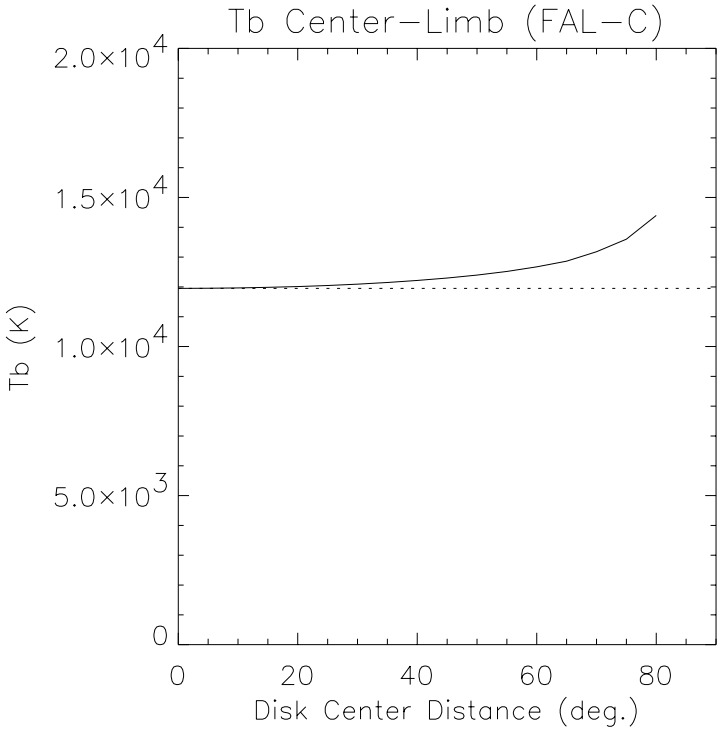

Fig. 2.. Center-to-limb brightness variation calculated at 17 GHz based on the FAL-C model (Fontenla et. al., 1993).

Sun.

NoRH has been operating since 1992. Observing frequencies are 17 GHz and 34 GHz (dual frequency mode after 1995). At 17 GHz, both right-handed-circular polarization (RCP) and left-handed-circular polarization (LCP) are received. Data of 17 GHz RCP, LCP and 34 GHz are taken nearly simultaneously or a time-sharing basis with a duty cycle of 100 ms. In normal mode, one second integrated data are stored. Daily observation is roughly from 2300 UT until 0700 UT, which depends on the season. Eight-hour continuous data sets are available daily since late June 1992. There is a long data gap from August to October in 1995 when 34 GHz receiving capability was installed. Opacity of the terrestrial atmosphere including clouds is small at 17 GHz. Even during cloudy or rainy days, we can observe the Sun. Only during heavy rain and wet snow pileup, NoRH cannot see the Sun. So the data coverage is very good.

Field of view of the element antennas covers the full disk of the Sun for both 17 GHz and 34 GHz. The diameter of the element antennas is 80 cm and the illumination at 34 GHz is limited only to the central part of the antenna to broaden the field of view. Attenuation of the primary beam near the solar limb is about 10 percent at 17 GHz. The array configuration of NoRH is an inverted Tee shape. East, West and North arms have 28 antennas each. Baseline length covers from 1.5 m to 245 m which determines the field of view of 40 arc min and the highest spatial resolution of 10 arc sec in 2-D at 17 GHz. In 1-D mode in E-W, the highest available spatial resolution is 5 arc sec. At 34 GHz, the field of view determined by the shortest baseline length is 20 arc min. Combined with the fact that the element antenna covers the whole solar disk, snap shot images at 34 GHz are a superposition of images at different parts of the solar disk. This does not influence much when we study bright features such as flares and active regions. However it is not good for the studies of the quiet sun. In the following, quiet sun studies are limited only to 17 GHz.

NoRH is a radio interferometer. It measures spatial Fourier components (visibilities) of the brightness distribution on the sky. The complex visibilities are cross correlation values of the output signals from pairs of antennas. The arguments of the measured visibilities are baseline vectors normalized by the observing wavelength. We are using the plane defined by the array as the reference plane for the baseline vectors. Solar images are projected on this plane and are deformed by the projection. The deformation is corrected after the image synthesis.

The antenna array of NoRH has a lot of redundancy. Antennas are populated densely near the array center and are sparsely populated outwards. They are located on the grid points. The redundancy is used for self-calibration of phases and amplitudes. Calibration data are taken simultaneously with the observations. However, positional information is lost in the process of self-calibration. We use the synthesized solar disk as the positional reference. The large number of short baselines is used for the synthesis of the reliable solar disk. As the locations of the antennas are on the regular grid points, there are many high sidelobes (or grating lobes). To suppress them, image restoration is inevitable after synthesis by the inverse Fourier transformation. We are using CLEAN for the restoration. As the high sidelobe level disturbs the weak features in the quiet regions, deep CLEANing is necessary. We are using the CLEAN algorithm proposed by Steer et al. (1984) to speed up the CLEAN process to realize deep CLEANing (Koshiishi, 1996). If the calibrations were perfect and there were no errors in measurements, we could expect high quality restored images. However, real situations are not so. We can see many scattered point-like sources, which change from image to image. We need further improvement of calibrations and other restoration methods such as MEM to suppress them. At present, we need to limit the reliable features to sources brighter than several percent of the quiet sun level. Or, carefully check the persistence or consistency of the interested features. Quiet sun level at 17 GHz is defined as 10,000 K based on the measurement by Zirin et al. (1991).

For the studies of faint features by NoRH, we synthesize radio images with broader beam with 18 arc second resolution. This is the result of natural weighting for the measured visibility to get high sensitivity.

6. Observed Quiet Sun Features

6.1. Fine structures

Studies of fine structures of the order of seconds or smaller, such as quiet sun networks, require greater resolution of a larger array. Bastian et al. (1996) used the VLA at 23 and 15 GHz for the quiet sun observations. The detected network structures coincide well with magnetic network structures. Their results were similar to that of the observations at longer wavelengths by Gary and Zirin (1988). Both studies and also the work by Gary et al. (1990) showed time variability of the network related features, but their variations did not necessarily coincide with that of the network magnetic features.

Krucker et al. (1997) and Benz et al. (1997) studied weak activities in the quiet sun by the VLA and SXT/YOHKOH. Long exposure of the quiet sun by SXT and VLA made it possible to detect weak activities in the magnetic networks. They refer to them as network flares. They found evidence for nonthermal emission associated with these activities. They discussed the possibility of coronal heating by these network flares.

6.2. Coronal Holes

Coronal holes are areas of weak coronal emission compared with the surrounding regions in soft x-ray and EUV. The magnetic field structures are open, hence plasma is not trapped by the magnetic fields. Of main importance of the studies of coronal holes is the fact that high velocity solar wind streams emanate from coronal holes. Studies of coronal holes attempt to find acceleration mechanisms of high velocity solar wind. Due to less emission, diagnostics of the coronal holes are extremely difficult. Hara et al. (1994) studied carefully the soft x-ray emission observed by the SXT/YOHKOH from the coronal hole by subtracting the influences from the surrounding bright area. They found that the temperature in the coronal hole does not differ from that of the normal quiet sun. However, their result is not conclusive. Further studies are going on (e.g. Foley et al., 1997).

Microwave observations of coronal holes pertain to the lower layers of the solar atmosphere within coronal holes. They are not darker than the surrounding quiet area, rather enhanced microwave emission can be found in some parts of coronal holes. Kosugi et al. (1986), and some earlier studies, pointed out this phenomenon. Gopalswamy et al. (1998) studied carefully the relation between the magnetic features in a coronal hole and the radio brightness distribution taken by NoRH. Magnetically enhanced regions in the coronal hole coincide with the brighter regions. The current image quality of the NoRH limits detailed comparisons of fine structures of weak radio features as is mentioned in section 5.

6.3. Radio Synoptic Maps and Polar Brightening

To study quiet features that last longer than weeks, synoptic methods can be very powerful (Shibasaki, 1998). Figure 3 shows a set of synoptic maps of one rotation: radio (NoRH), soft x-ray (SXT/YOHK), and magnetic field (KPNO). In these synoptic maps, one can immediately see the following characteristics: 1) Some parts of coronal holes are brighter in radio. 2) Radio dark filaments well follow the magnetic polarity reversal line (often better than

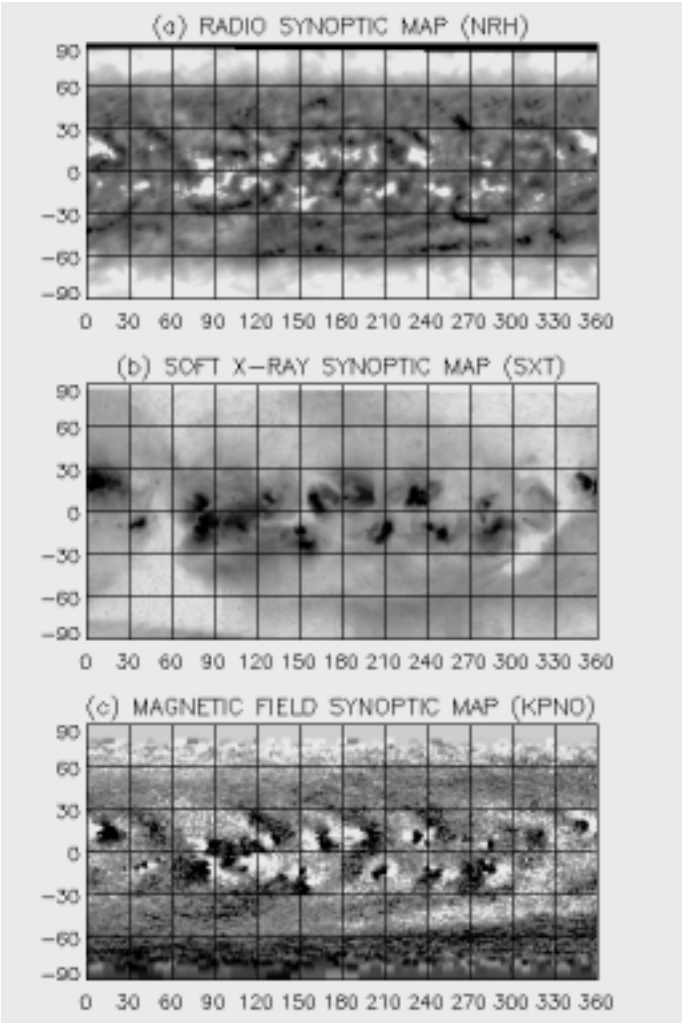

Fig. 3.. A set of synoptic maps of the Carrington rotation 1868 (Shibasaki, 1998): (a) Radio synoptic map by the NoRH. $9,000K \leq T_b \leq 12,000K$, (b) Soft x-ray synoptic maps (SXT/YOHKOH), and (c) Photospheric magnetic field (KPNO).

H-α dark filaments). 3) The most striking feature in the radio synoptic map is that both polar regions are brighter than lower latitude regions. This phenomenon is called "polar cap brightening" (Kosugi et al., 1986). The "polar cap brightening" is only detected in short-cm/mm (Pohjolainen et al., 1999) wavelengths. It is not detected in other wavelengths including EUV, soft x-ray and optical. Shibasaki (1998) showed that the polar cap brightening consists of two components, one is fixed to the polar region, and the other is a limb brightening effect. The B_o dependence and independence of the polar cap brightening can separate these two components (Koshiishi, 1996, and Shibasaki,

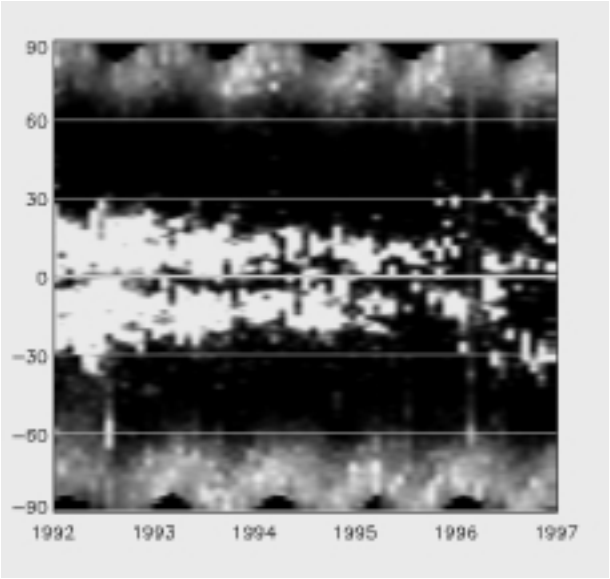

Fig. 4.. 4. A radio butterfly diagram from July 1992 to July 1997 synthesized from the radio synoptic maps of the NoRH.

1998). Open magnetic field structure in the polar region at the height of the upper chromosphere may somehow be related to the cause of the polar cap brightening. Less enhancement in low latitude limb than predicted may be explained by the supression of the limb brightening due to low lying closed magnetic field filled with low temperature plasma. It is also found that the polar cap brightening area expands as the solar activity declines. This can be found in the radio butterfly diagram shown in Figure 4 (Shibasaki, 1998).

Importance of the polar region studies derives from the importance of coronal holes. Recent Ulysses observations of solar wind rediscovered high velocity flows at high latitude regions (McComas, D.J. et al, 1998). The three-station radio scintillation method of measuring solar wind velocity from the ground had already shown them (Kojima and Kakinuma, 1990). Search for the extra acceleration of solar wind velocity is the one motivation of the polar region studies. Extensive studies of polar regions are underway by SoHO (e.g. DeForest, C.E. et al, 1997). Comparisons are being made of compact bright features in polar regions found by NoRH with polar plumes observed by SoHO and with polar faculae observed by white light.

6.4. Other features

Dark filaments and prominences are well observed in microwave regions at shorter wavelengths. Filaments on the disk are normally observed as absorption, while the prominences are seen in emission against the sky background. Studies of filaments and prominences are related to their eruptions. Their eruptions are associated with larger-scale magnetic eruptions called CMEs. The NoRH is also a good instrument to detect prominence eruptions. This subject is discussed extensively in other parts of this issue.

The NoRH always observes weak and compact transient sources on the disk. Time series of one-dimensional (E-W) images (without any image restoration processes) show life times of about half an hour and rather uniform distribution over the disk. Identification of these features needs high dynamic range two-dimensional images. For the energetics of these features, other information is needed such as EUV and soft x-ray. This is an interesting subject for future studies.

7. Summary and Future Direction

In this review, radio emission (thermal free-free mechanism) from the quiet sun and atmospheric models of the quiet sun are summarized. Frequency spectrum of the radio brightness temperature calculated using the models are compared with the observations. It is shown that the FAL model is very close to the observation compared to

the previous VAL model. Then the performances and limitations of the Nobeyama Radioheliograph for the studies of quiet sun are summarized and observed features of the quiet sun by NoRH and other telescopes are reviewed. Coronal holes, polar cap brightening are interesting subjects for further studies. It is shown that the NoRH is a powerful tool for quiet sun studies.

Radio telescopes currently available for the studies of quiet sun are NoRH, VLA and large single dishes operating at shorter wavelengths (millimeter and sub-millimeter). This situation will not change quickly. In the future, large arrays operating at sub-millimeter will be used for study of the quiet sun for the diagnostics of the low layers of the solar atmosphere and will be able to improve the model.

By further improving phase / amplitude calibrations and image synthesis / restoration methods of NoRH, higher dynamic range images of the quiet sun will be available. This will open other possibilities of research, which cannot be done with the current image quality.

References

Avrett, E. H., in "Infrared Tools for Astrophysics" Eds., Kuhn, J. R., and Penn, M. J., World scientific, Singapore, 303
Bastian, T., Dulk, G. A. and Leblanc, Y., ApJ., 473, 539, 1996
Benz, a. O., et al., A&A, 320, 993, 1997.
DeForest, C. E. et al., Solar Phys., 175, 393, 1997
Dulk, G. A., ARA&A, 23, 169, 1985
Foley, C. R. et al., ApJ, 491, 933, 1997
Fontenla, J. M., Avrett E. H., and Loeser, R., ApJ., 406, 319, 1993 (FAL model)
Gary, D. E., and Zirin, H., ApJ, 329, 991, 1988
Gary, D. E., Zirin, H. and Wang, H., ApJ, 355, 321, 1990
Gopalswamy et al., ASP Conf. Ser., 140, 363, 1998
Hara, H., et al., PASJ, 46, 493, 1994
Kojima, M. and Kakinuma, T., Space Sci. Rev., 53, 173,1990
Koshiishi, H., Doctoral Thesis, University of Tokyo, 1996
Kosugi, T., Ishiguro, M. and Shibasaki, K., PASJ, 38, 1, 1986
Krucker, S. et al, ApJ., 488, 499, 1997
Lindsey, C. et al., ApJ., 453, 511, 1995
McComas, D. J. et al., Geophys. Res. Lett, 25, 1, 1998
Nakajima, H. et al., Proc. IEEE, 82, 705, 1994
Pohjolainen, S., Portier-Fozzani, F. and Ragaigne, D., this issue.
Shibasaki, K., ASP Conf. Ser, 140, 387, 1998
Steer, D. G., Dewdney, P. E. and Ito, M. R., A&A, 137, 139, 1984
Vernazza, J. E., Avrett, E. H. and Loeser, R., ApJ Sup., 45, 635, 1981 (VAL model)
Zirin, H., Baumert, B. M. and Hurford, G. J., ApJ., 370, 779, 1991